ACS OMEGA

http://pubs.acs.org/journal/acsodf

Article

Ultrasound-Assisted Adsorption of Perchlorate Using Calcined Hydrotalcites and the Thermal Stabilization Effect of Recycled Adsorbents on Poly(vinyl chloride)

Changwei Cui, Youhao Zhang, Michael A. Wladyka, Tianyu Wang, Weifeng Song,* and Kangmin Niu*

Cite This: *ACS Omega* 2023, 8, 17689−17698

Read Online

ACCESS | Metrics & More | Article Recommendations

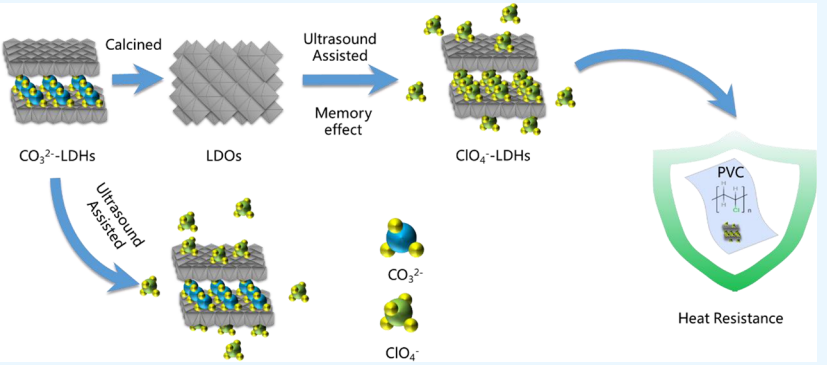

ABSTRACT: Due to their high anion exchange and memory effect, the layered double hydroxides (LHDs) have wide applications for some areas. In this work, an efficient and green recycling route for layered double hydroxide based adsorbents is proposed specifically for application as a poly(vinyl chloride) (PVC) heat stabilizer without requiring secondary calcination. Conventional magnesium−aluminum hydrotalcite was synthesized using the hydrothermal method followed by removal of carbonate anion (CO_3^{2-}) between LDH layers by calcination. The adsorption of perchlorate anion (ClO_4^-) by the memory effect of calcined LDHs with and without ultrasound assistance was compared. Using ultrasound assistance, the maximum adsorption capacity of the adsorbents (291.89 mg/g) was increased, and the adsorption process was fitted using the kinetic Elovich rate equation (R^2 = 0.992) and Langmuir adsorption model (R^2 = 0.996). This material was characterized using XRD, FT-IR, EDS, and TGA which demonstrated that ClO_4^- was intercalated into the hydrotalcite layer successfully. The recycled adsorbents were used to augment a commercial calcium−zinc-based PVC stabilizer package applied in a epoxidized soybean oil plasticized cast sheet which is based on an emulsion type PVC homopolymer resin. Use of perchlorate intercalated LDH augmentation yielded significant improvement to static heat resistance as indicated by the degree of discoloration with a life extension of approximately 60 min. The improved stability was corroborated by evaluation of HCl gas evolved during thermal degradation using conductivity change curves and the Congo red test.

1. INTRODUCTION

In recent years, perchlorate (ClO_4^-) as an emerging trace contaminant has been detected in water and soil resources, as well as foods, and can influence the thyroid's uptake of iodide, resulting in the dysfunction of certain metabolic processes.[1−4] The use of perchlorate is mostly related to military and aerospace activities, such as oxidizers in solid fuel rocket propellants, explosives, and pyrotechnics.[5−7] Perchlorate is widely regarded as a persistent pollutant in groundwater and surface water due to its high solubility, nonreactivity, and nonvolatility.[8] Various approaches including physical, chemical, and biological treatments and combination technologies have been developed for the removal of perchlorate.[9−12] Considering cost effectiveness and treatment efficiency, the adsorption process is very attractive for water treatment.[13−15] Hydrotalcites also known as layered double hydroxides (LDHs, $[M_{1-x}^{2+}M_x^{3+}(OH)_2][A_{x/n}^{n-}\cdot mH_2O]$), are high-performance adsorbents used to remove anions[16,17] and also have application prospects as antibacterial agents,[18] flame retardants,[19] anticorrosion agents,[20] drug delivery vehicles,[21] stabilizers,[22] solar cell components,[23] pollutant removal

Received: January 10, 2023
Accepted: March 9, 2023
Published: May 9, 2023

https://doi.org/10.1021/acsomega.3c00176
ACS Omega 2023, 8, 17689−17698

materials,[24] catalysts,[25] and sensors.[26] They are a class of inorganic material with a layered structure that contain positive charges balanced by the intercalation of anions in the hydrated interlayer regions which have specific surface area and high interlayer anion mobility.[27,28] Three mechanisms work in the uptake of anions by LDHs from water:[29] (a) surface physical adsorption; (b) anion exchange; (c) reconstruction by anion intercalation after calcining. Generally, high-valent anions are easily exchanged into the interlayer while low-valent anions are easily exchanged out, which means physical effects will dominate the adsorption of ClO_4^- by LDHs.[30] However, it is difficult to achieve efficient contaminant conversion only by physical adsorption in LDHs; therefore further treatment is required.[31]

Memory effect is the restoration of the original LDH structure by rehydration, applying decarbonation and subsequent reconstruction utilizing target anionic groups.[32−34] By this effect, both harmful organic and inorganic anions from wastewater can be intercalated into the interlayer and removed successfully.[35,36] Yang et al.[37] synthesized a novel material of calcined iron-based LDH for ClO_4^- adsorption from water using a co-precipitation method. In this study, ClO_4^- at 2000 μg/L concentration was almost all adsorbed within 720 min by 1.33 g/L MgFe-3CLDH (calcination temperature = 550 °C and [Mg]/[Fe] = 3) at 25 °C and initial solution pH of 4−10. Lin et al.[38] reported that the high ClO_4^- adsorption capacity (279.6 mg/g) of the calcined LDH was mainly driven by the structural memory effect. In addition, they proposed that the negative charge of ClO_4^- was transferred to positively charged hydroxide layers via electrostatic interactions, and then strong hydrogen bonds were formed between the oxygen atoms of ClO_4^- polarized by the surrounding hydroxyls in the hydroxide layers. In Liu's study, the calcined Mg/Fe hydrotalcite (CHT) and hydrotalcite-based Pd/Co catalyst (Pd/Co-CHT) were prepared and utilized to adsorb and reduce the ClO_4^- in water. Results indicated that the removal efficiency of two processes involving the adsorption and reduction for the hydrogen reduction of ClO_4^- by Pd/Co-CHT was 3 times higher than that of a single adsorption process.[39]

In order to enhance the adsorption efficiency of calcined hydrotalcite, it had been reported that ultrasonic energy can be applied to improve adsorption of small molecules.[40−42] This positive effect is attributed to ultrasonic cavitation. When ultrasonic cavitation occurs a bubble of vacuum is formed which rapidly collapses exerting extremely high pressure and releasing a large amount of energy. This energy may reduce the diffusion resistance and facilitate the entry of anions into the interlayer space and ultimately enhance the uptake capacity.[43−45] It was found in Iglesias's experiment that the utilization of ultrasound resulted in a 2-fold increase in the adsorption capacity of the sample, which suggested that both the diffusion and transfer of anions were boosted by ultrasound, resulting a more efficient technique for water remediation.[46] Zhang et al.[47] reported that the adsorption equilibrium time of $MgAlCO_3$ LDH and Congo red was shortened from 5 to 2 h under ultrasound-assisted adsorption, and the removal efficiency of the dye was also much higher than that of other processes. In another study, Szabados et al.[48] successfully intercalated halide ions (except fluoride) and oxo anions into CaFe-LDH by sonication, which is difficult to achieve with other methods. Although advantages for the efficiency and capability of LDHs when combined with sonication has been demonstrated in this work relatively little advancement has been achieved in this field.[49]

In addition, the research on the recycling and reuse of adsorbents has great significance in regards to the sustainability of resources.[50−53] However, most techniques adopt the decomposition−reconstruction cycle route requiring calcined LDH, which undoubtedly increased the carbon emission.[33,54,55] Meanwhile, the adsorption rate of LDHs after secondary calcination is greatly decreased, leading to low utilization.[56−58] In fact, LDHs as highly efficient and environmentally friendly PVC thermal stabilizers have been used widely.[59−62] The alkalinity of LDHs can directly neutralize HCl reducing the autocatalytic effect; however the Cl^- ion can also exchange into the interlayer though interaction with the interlayer guest and form Cl^- intercalated LDHs further inhibiting the chain degradation reaction.[63−66] The service life of petroleum-based PVC can be extended with LDHs, which reduce the use of petroleum components and enhance sustainability. Thus far, no investigation exploring application of recovered LDHs as a PVC thermal stabilizer has been conducted, especially for ClO_4^- intercalated hydrotalcites.[30,31,67,68]

Here we evaluate the capability of calcined LDHs to adsorbed ClO_4^- in wastewater utilizing sonication with subsequent evaluation of recovered ClO_4^--LDH for efficacy as a PVC stabilizer. The most prevalent Mg−Al-LDH was synthesized and calcined to endow it with the ability to intercalate anions. The adsorption efficiency of ultrasound-assisted vs standard vibration alone was compared. The chemical and physical properties of LDH, LDO, and reconstructed ClO_4^--LDH were characterized. Finally, the recycled adsorbents as auxiliary thermal stabilizer were added into PVC together with the Ca−Zn base stabilizer to research the thermal stability.

2. EXPERIMENTAL SECTION

2.1. Chemicals. Magnesium chloride hexahydrate ($MgCl_2·6H_2O$) and aluminum chloride hexahydrate ($AlCl_3·6H_2O$) were supplied by Damao Chemical Reagent Factory (China). Sodium hydroxide (NaOH) and sodium carbonate (Na_2CO_3) were provided by Beijing Tong Guang Fine Chemical Co., Ltd. (China). Sodium perchlorate ($NaClO_4$) was obtained from Sigma-Aldrich (Shanghai) Trading Co. Ltd. PVC was prepared by Vinnolit GmbH & Co. KG, Germany. Epoxidized soybean oil (ESO) was purchased from Nanjing Rongji Chemical Co., Ltd. Zinc stearate ($(Zn(St)_2)$) and calcium stearate ($Ca(St)_2$) were supplied by Transfar Chemistry. All of the reagents were of analytical purity and were used directly.

2.2. Synthesis of Mg−Al-LDH and Mg−Al-LDO. Mg−Al-LDH was synthesized by a conventional co-precipitation method at constant pH. The $MgCl_2·6H_2O$ and $AlCl_3·6H_2O$ at 2 M ratio were dissolved in 100 mL of deionized water, and the total ion concentration was 1 mol/L. The mixed solution was added to a three-necked flask and stirred vigorously. The precipitant solution was composed of 1 mol/L NaOH and 0.1 mol/L Na_2CO_3 blended in 100 mL of deionized water. The precipitant solution was added drop-by-drop in the three-necked flask at 60 °C with a constant pressure funnel and stirred vigorously. The pH of the whole precipitation process was maintained at about 10 by adding appropriate volumes of NaOH. The formed precipitate was kept at 80 °C for 24 h and then washed 3 times with deionized water under reduced pressure filtration. The collected precipitates were vacuum-

https://doi.org/10.1021/acsomega.3c00176
ACS Omega 2023, 8, 17689−17698

dried at 60 °C for 6 h, and then ground to obtain layered double hydroxide, Mg−Al-LDH (CO_3^{2-}-LDH). CO_3^{2-}-LDH was calcined in a muffle furnace at 500 °C for 4 h to obtain Mg−Al-LDO (LDO).

2.3. Ultrasound-Assisted Adsorption of ClO_4^-. Contaminated water sources were simulated with a $NaClO_4$ aqueous solution. 2 g/L of the LDO (LDH) was added to 100 mL of $NaClO_4$ aqueous solution with an initial concentration of 100 mg/L. The adsorption kinetics experiments were carried out in an ultrasonic bath with a frequency of 40 kHz and a constant temperature of 25 °C, and the sampling times were 2 h, 4 h, 6 h, 8 h, 10 h, and 12 h. The collected supernatant was filtered through a 0.2 μm nylon syringe filter prior to ion chromatography (IC) analysis. After the adsorption, the adsorbents at 12 h adsorption time were recovered by centrifugation, washed with deionized water, dried, and then characterized and tested as stabilizers. In addition, the adsorption isotherms of ClO_4^- adsorption by the LDO (LDH) were investigated at initial ClO_4^- concentrations of 5, 10, 20, 50, 100, 200, 300, 400, and 500 mg/L at the same adsorption conditions. 0.2 g of LDO (LDH) was added to 100 mL of ClO_4^- solution in a conical flask, and the suspensions were placed in the ultrasonic bath for several minutes until equilibrium was achieved. The supernatant was obtained by filtration. As a control, another set of adsorption experiments was performed on a mechanical vibration table with a constant temperature of 25 °C and a vibration frequency of 300 rpm. The adsorption of ClO_4^- by LDO (LDH) under ultrasonic assistance was denoted as U-LDO (U-LDH), and the adsorption process under the vibration table method was represented as S-LDO (S-LDH). The pH of the mixture was not controlled in order to avoid introducing other anions.

The perchlorate concentration in the supernatant was analyzed using an ion chromatography (IC) system (ICS-600, Thermo Fisher, USA) that was equipped with an AS-AP autosampler, AS-16 analytical column, AG-16 guard column, and 10 μL sample loop. ClO_4^- detection was achieved using a 60 mM KOH eluent flowing at 1.0 cm^3/min at 30 °C. The detection limit of ClO_4^- was 0.05 mg/L. In the adsorption equilibrium evaluation, Langmuir and Freundlich isotherms were assessed to fit the experimental data by model eqs 1 and 2, respectively.

Langmuir model:

$$q_e = \frac{Q_0 C_e K_L}{1 + C_e K_L} \tag{1}$$

Freundlich model:

$$q_e = K_F C_e^{\,n} \tag{2}$$

where q_e is the amount of adsorbed ClO_4^- per mass unit LDO at equilibrium (mg/g), C_e is the equilibrium concentration of ClO_4^- solution at adsorption equilibrium (mg/L), Q_0 is the saturated monolayer adsorption capacity (mg/g), K_L is the Langmuir-related adsorption capacity parameter (L/mg), K_F is the Freundlich model-related isotherm parameter, and n is the adsorption intensity. In the adsorption kinetic evaluation, three common kinetics models were used for analysis:

pseudo-first-order model:

$$Q_t = Q^\theta(1 - e^{-k_1 t}) \tag{3}$$

pseudo-second-order model:

$$Q_t = Q^\theta\left(1 - \frac{1}{k_2 Q^\theta t + 1}\right) \tag{4}$$

Elovich model:

$$Q_t = \frac{1}{\beta}\ln(\alpha\beta t + 1) \tag{5}$$

where Q_t and Q^θ are the adsorption loadings of ClO_4^- on the LDO (mg/g) at time t (min) and at equilibrium, k_1 and k_2 are the rate constant of adsorption (min^{-1}), α represents the initial adsorption rate constant (mg/(g·min)), and β is a constant related to adsorbent surface coverage and chemisorption activation energy (g/mg).

2.4. Preparation of LDH−PVC Composites. The contents and names of the PVC composites are shown in Table 1. The stabilizer package was first dispersed in the plasticizer ESO followed by addition of the PVC resin. The dispersion power was 750 W, and stirring was maintained for 15 min; then the mixture was degassed by mixing under vacuum for 2 h. PVC films were cast using a knife-over-roll laboratory coater onto a commercial release paper substrate using a knife gap distance of 1 mm. The fusion temperature was 180 °C, and time was 1 min. The prepared PVC sheets were cut into 3 × 3 cm^2 samples for subsequent thermal stability test.

Table 1. Formulation of PVC Composites[a]

			stabilizer package			
sample	PVC	ESO	$Ca(St)_2$	$Zn(St)_2$	CO_3^{2-}-LDHs	ClO_4^--LDHs
PVC	100	50				
Ca/Zn-PVC	100	50	1.2	0.4		
CO_3^{2-}-LDH−Ca/Zn-PVC	100	50	1.2	0.4	1	
ClO_4^--LDH−Ca/Zn-PVC	100	50	1.2	0.4		1

[a]Amount of components given in grams.

2.5. Characterization of Adsorbents. The physical parameters of adsorbents including specific surface area, average pore volume, and pore diameter were surveyed by the Brunauer−Emmett−Teller (BET) method using a specific surface area analyzer, Kubo1200. The crystal structure of CO_3^{2-}-LDH, LDO, and ClO_4^--LDH was characterized with a Rigaku D/Max 2550/PC diffractometer. The scanning range was from 5° to 90° with a step size of 0.02° 2θ. The FTIR spectra of the anion-exchange in the LDH interlayer was recorded in the range of 4000−400 cm^{-1} with a resolution of 1.0 cm^{-1} by a Nicolet IS10 spectrometer. The SEM of CO_3^{2-}-LDH, LDO, and reconstructed CO_3^{2-}-LDH was observed using a HITACHI S-4800 field-emission scanning electron microscope. TG-DTA measurements were performed on a Netsch STA449C thermal gravimetric analyzer from room temperature to 800 °C at a heating rate of 10 °C/min in air.

2.6. Evaluation of LDH−PVC Sheet. The thermal stability in a series of LDH−PVC sheets was evaluated based on discoloration and dehydrochlorination. The discoloration evaluation was performed in accordance with ISO 305:1990-4. Thermal aging of cast sheets was performed in forced air oven at 180 °C. The monitoring time interval of the samples was 10

https://doi.org/10.1021/acsomega.3c00176
ACS Omega 2023, 8, 17689−17698

min. Discoloration was appraised by the ΔL^*, ΔA^*, and ΔB^* values, which were determined using an Xrite Color-Eye 7000A type automatic color difference meter. Among them, the ΔL^*, ΔA^*, and ΔB^* values displayed by the color meter stood for white (+) and black (−), red (+) and green (−), and yellow (+) and blue (−), respectively. The CIE-$L^*A^*B^*$ values could be used to formulate a value for total change as ΔE by the following equation:

$$\Delta E = \sqrt{(\Delta L^*)^2 + (\Delta A^*)^2 + (\Delta B^*)^2} \quad (6)$$

This value was used to describe the discoloration of LDH−PVC composites, and a low value corresponds to a low color difference.

The dehydrochlorination was preformed according ISO 182-2:1990-12. 2.0 ± 0.05 g mass of PVC composites were cut into many small pieces with sides approximately 2 mm long. The HCl released during degradation at 180 °C was purged with N_2 at a rate of 7 L/h and trapped in 100 mL of deionized water at room temperature. The process of the decomposition was tracked by monitoring the change in the conductivity of water. Either the induction time (i.e., the time required to reach the break point of the curve) or the stability time (i.e., the time to reach a conductivity difference of 50 μS/cm) was used to quantify performance.

3. RESULTS AND DISCUSSION

In Table 2, the specific surface area and the corresponding pore size distribution of the original LDH and calcined LDH, which were investigated by using N_2 adsorption−desorption measurements, are reported. Compared with the original LDH, the calcined hydrotalcite had larger pore volume (0.78 cm^3/g) and average pore size (18.8 nm), but the specific surface area was reduced to 138.6 m^2/g. Larger pore volume and pore size are more favorable for the adsorption of large-diameter ClO_4^- anion groups. The lower BET specific surface area was due to the collapse of pore structure and the increase of agglomeration after calcination.[69] The morphology of the hydrotalcite before and after calcination is shown in the SEM images. The common hexagon shape in CO_3^{2-}-LDH and the staggered appearance of the LDO are shown clearly in Figure 1. It could be seen that the LDH prepared by the hydrothermal method had a good layered structure and dispersibility, and the particle size was about 400 nm. After calcination, the hydrotalcite exhibited a remarkable phenomenon with collapse of the layered structure accompanied with severe agglomeration, which supports the same conclusion as the BET specific surface area analysis. In addition, the hydrotalcite reconstructed by the memory effect still had layered structure from the SEM image; however the agglomerates did not disperse under ultrasonic assistance and the phenomenon of "clumping" still existed. It could be seen from the EDS analysis that the synthesized CO_3^{2-}-LDH had a magnesium−aluminum ratio of 2.17, and the presence of Cl element in the reconstructed hydrotalcite verified the intercalation of perchlorate.

Table 2. Textural Parameters of CO_3^{2-}-LDH and LDO

sample	S_{BET} (m^2/g)	pore volume (cm^3/g)	pore diameter (nm)
CO_3^{2-}-LDH	145.7	0.36	13.2
LDO	138.6	0.78	18.8

To investigate the relevant adsorption mechanism, the relationship between the equilibrium concentration (C_e) and the equilibrium adsorption capacity (q_e) was determined by the adsorption isotherm upon reaching adsorption equilibrium. Figure 2 displays the equilibrium isotherms of ClO_4^- taken up by CO_3^{2-}-LDH and LDO. Two common isotherm models (Langmuir and Freundlich isotherm models) were used to fit the experimental data. For the adsorption isotherms of CO_3^{2-}-LDH, the results of the Freundlich equation fit were more consistent with the experimental data, and the model parameters are listed in Table 3. It could be seen that only a trace of ClO_4^- was adsorbed by the CO_3^{2-}-LDH, and a large amount of ClO_4^- still existed in the aqueous phase.[38] At this time, the adsorption of ClO_4^- only occurred in the hydration layer on the surface of the plate without ion exchange with CO_3^{2-} through the memory effect. The two almost coincident isotherms indicated that ultrasound assistance provided no significant improvement in the process of adsorption of perchlorate by CO_3^{2-}-LDH, and the CO_3^{2-}-LDH under both ultrasound-assisted and mechanical agitation exhibited a low level removal efficiency of ClO_4^-. In contrast, the LDO after the decomposition of the CO_3^{2-} by calcination exhibited a much stronger adsorption with ClO_4^- than the corresponding parent LDH. The adsorption isotherms of ClO_4^- were well fitted by the Langmuir model, which distinctly displayed a nonlinear adsorption. The model parameters are listed in Table 3. The ultrasound-assisted adsorption of LDO had much larger capacity coefficient Q_0 (291.89 mg/g) and adsorption rate coefficient K_L (0.0184) than that of mechanical vibration,

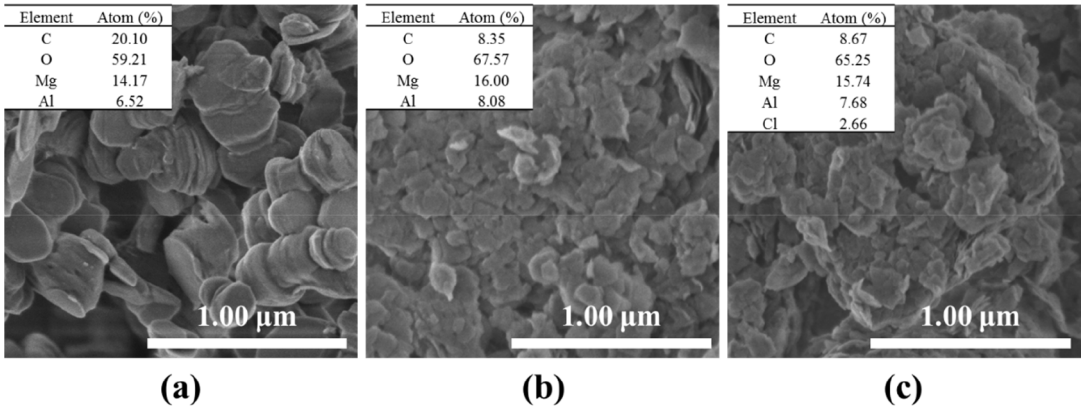

Figure 1. SEM images and element contents of (a) CO_3^{2-}-LDH, (b) LDO, and (c) ClO_4^--LDH.

https://doi.org/10.1021/acsomega.3c00176
ACS Omega 2023, 8, 17689−17698

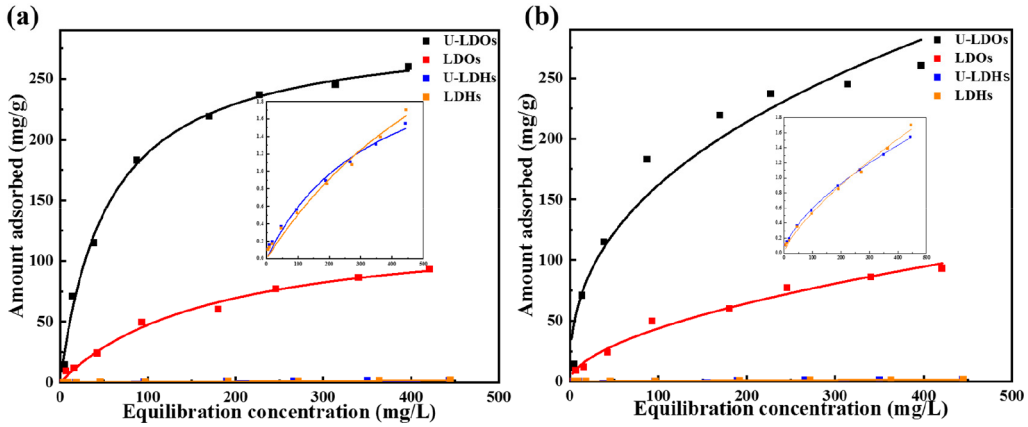

Figure 2. Adsorption isotherms of ClO_4^- onto original LDH and LDO with ultrasound assisted method and mechanical vibration method: (a) Langmuir model and (b) Freundlich model.

Table 3. Adsorption Isotherm Parameters of U-LDO, S-LDO, U-LDH, and S-LDH

	Langmuir equation			Freundlich equation		
	Q_0 (mg/g)	K_L (L/mg)	R^2	K_F	n	R^2
U-LDO	291.89 ± 6.83	0.0184 ± 0.0016	0.996	25.553 ± 7.1407	0.4010 ± 0.0513	0.947
S-LDO	130.03 ± 9.11	0.0057 ± 0.0010	0.990	3.392 ± 0.8534	0.5556 ± 0.0445	0.981
U-LDH	2.67 ± 0.34	0.0029 ± 0.0007	0.986	0.032 ± 0.0020	0.6324 ± 0.0003	0.999
S-LDH	4.63 ± 1.40	0.0012 ± 0.0005	0.982	0.018 ± 0.0037	0.7410 ± 0.0358	0.994

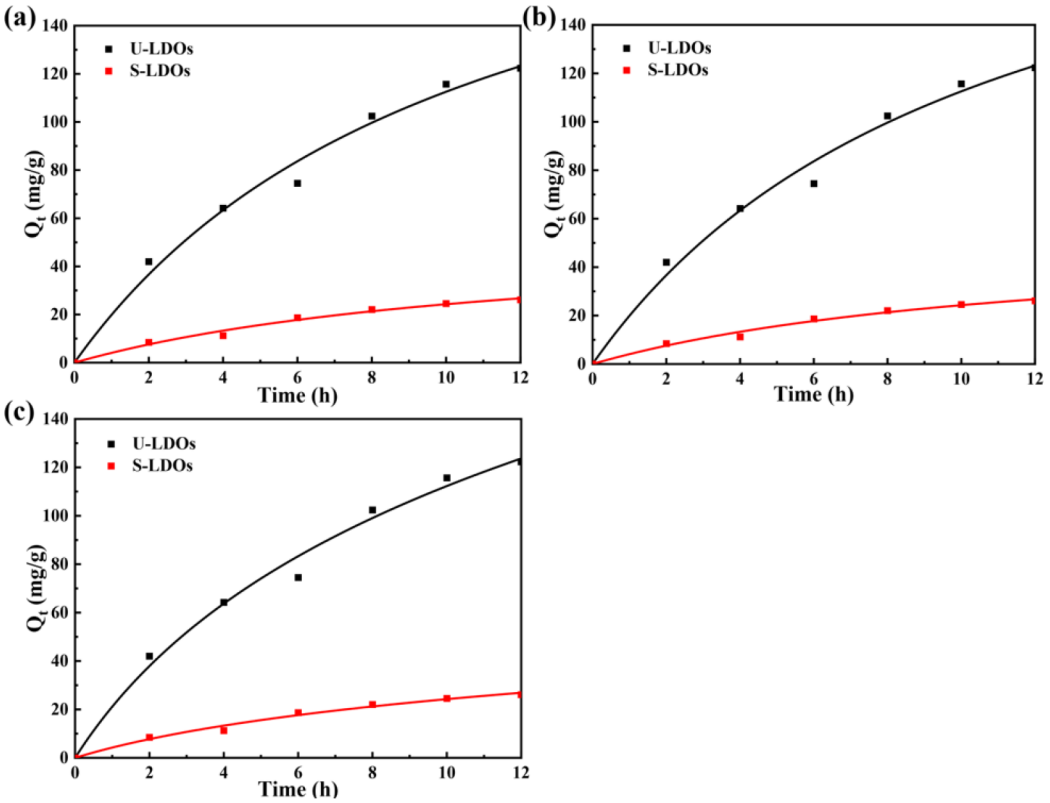

Figure 3. Adsorption kinetics of ClO_4^- onto the LDO with ultrasound assisted method and mechanical vibration method: (a) pseudo-first-order model, (b) pseudo-second-order model, and (c) Elovich model.

suggesting that ultrasound had an obvious positive effect on ion exchange between LDH layers.

The adsorption kinetics of ClO_4^- on LDO by different methods are shown in Figure 3. It could be seen from the figure that all the adsorption methods demonstrated a rapid adsorption process first, and then the adsorption rate decreased until it reached equilibrium. The fitting results and corresponding kinetic parameter values are shown in Table 4. Among the models, the fitting results of the Elovich kinetics model had the highest R^2 value, indicating that the adsorption

https://doi.org/10.1021/acsomega.3c00176
ACS Omega 2023, 8, 17689−17698

Table 4. Kinetics Parameters for ClO_4^- Adsorption by U-LDO and S-LDO

model	parameter	U-LDO	S-LDO
pseudo-first-order	Q^θ (mg/g)	156.20 ± 17.66	34.89 ± 4.18
	k_1 (min^{-1})	0.128 ± 0.026	0.120 ± 0.025
	R^2	0.985	0.986
pseudo-second-order	Q^θ (mg/g)	233.39 ± 33.38	54.06 ± 9.00
	$k_2 \times 10^{-4}$ (g/(mg·min))	3.99 ± 1.58	15.10 ± 6.75
	R^2	0.986	0.985
Elovich	α (mg/(g·min))	24.12 ± 3.46	4.73 ± 0.73
	β (g/mg)	0.012 ± 0.002	0.050 ± 0.012
	R^2	0.992	0.990

process of ClO_4^- to LDO was heterogeneous. That was a result of the combined action with multiple adsorption mechanisms rather than only one.[70,71] The β value changed from 0.050 g/mg to 0.012 g/mg when using ultrasound assistance, which was attributed to cavitation effects.

Figure 4a,b presents the FTIR spectra of the initial CO_3^{2-}-LDH and the LDO obtained after calcination, respectively.

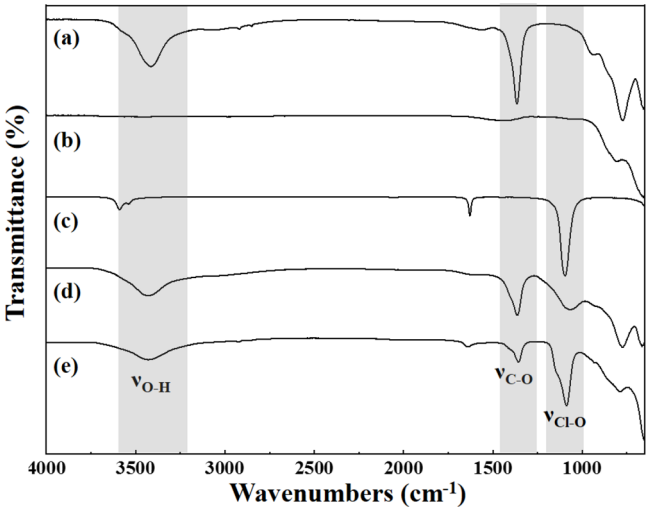

Figure 4. FTIR spectra of the CO_3^{2-}-LDH (a), LDO (b), $NaClO_4$ (c), S-ClO_4^--LDH (d), and U-ClO_4^--LDH (e).

Compared with the initial LDH, the characteristic absorption band of C−O at 1367 cm^{-1} and O−H at 3412 cm^{-1} for LDO disappeared, which indicated that H_2O and CO_3^{2-} ions in the LDH interlayer were eliminated after calcination. For the reconstructed S-ClO_4^--LDH and U-ClO_4^--LDH, a strong peak at 1000−1250 cm^{-1} assigned to Cl−O vibration was shown, which was verified by the FTIR spectra of sodium perchlorate shown in Figure 4c. The peaks displayed evident broadening, which was interpreted as the formation of hydrogen bonds of ClO_4^- with the surrounding water and hydroxyl groups in the interlayers.[72] Additionally, the Cl−O band exhibited a red shift from 1096 to 1088 cm^{-1} and 1062 cm^{-1}, caused by the inhomogeneous charge transfer in LDH layers. Both S-ClO_4^--LDH and U-ClO_4^--LDH showed a strong band at 1365 cm^{-1} originating from the asymmetric stretching of CO_3^{2-} owing to the absorption of carbonate formed by dissolving CO_2 in water. In contrast, the Cl−O characteristic absorption band of U-ClO_4^--LDH was more obvious than that of S-ClO_4^--LDH, suggesting that ultrasonic assistance improved the adsorption efficiency of LDO for ClO_4^-.

Figure 5 displays the XRD patterns of CO_3^{2-}-LDH, LDO, and ClO_4^--LDH. Sharp and symmetric peaks at (003) and

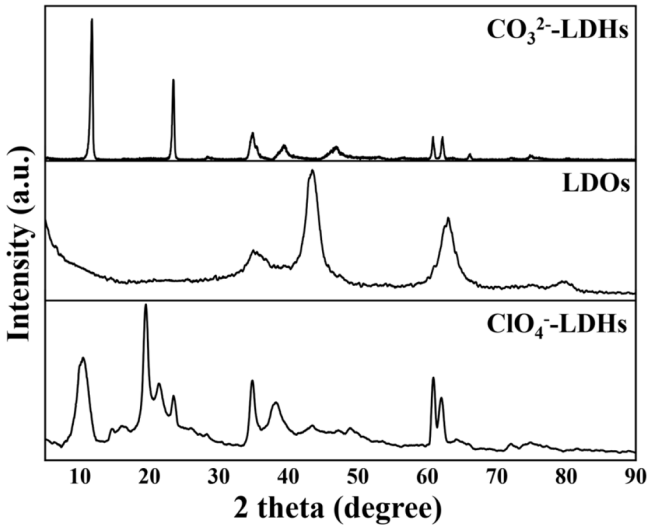

Figure 5. XRD spectra of CO_3^{2-}-LDH, LDO, and ClO_4^--LDH.

(006) basal planes were observed in the diffraction pattern of CO_3^{2-}-LDH, which are the characteristic reflections of layered double hydroxides. The layer structure of LDO was destroyed after calcination, leading to the formation of mixed magnesium−aluminum oxide, corroborated by the XRD pattern in which diffraction peaks of the layered hydrotalcite-like structure were absent. Upon adsorption of ClO_4^-, the ClO_4^--LDH again exhibited the characteristic diffraction peaks of LDH, indicating that the layer structure was reconstructed by rehydration due to the memory effect. In addition, the basal space of reconstructed adsorbents was 0.91 nm, larger than that for CO_3^{2-}-LDH (0.76 nm). This suggested the formation of ClO_4^--LDH.

The thermal behaviors of the CO_3^{2-}-LDH and ClO_4^--LDH were analyzed through TG-DTA experiments (Figure 6). Under two continuous mass loss steps, a major mass loss of

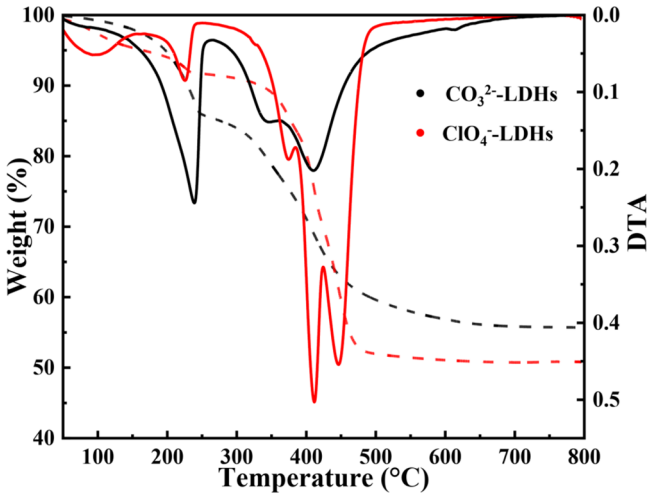

Figure 6. TGA (solid line) and DTA (dotted line) spectra of CO_3^{2-}-LDH and ClO_4^--LDH.

https://doi.org/10.1021/acsomega.3c00176
ACS Omega 2023, 8, 17689−17698

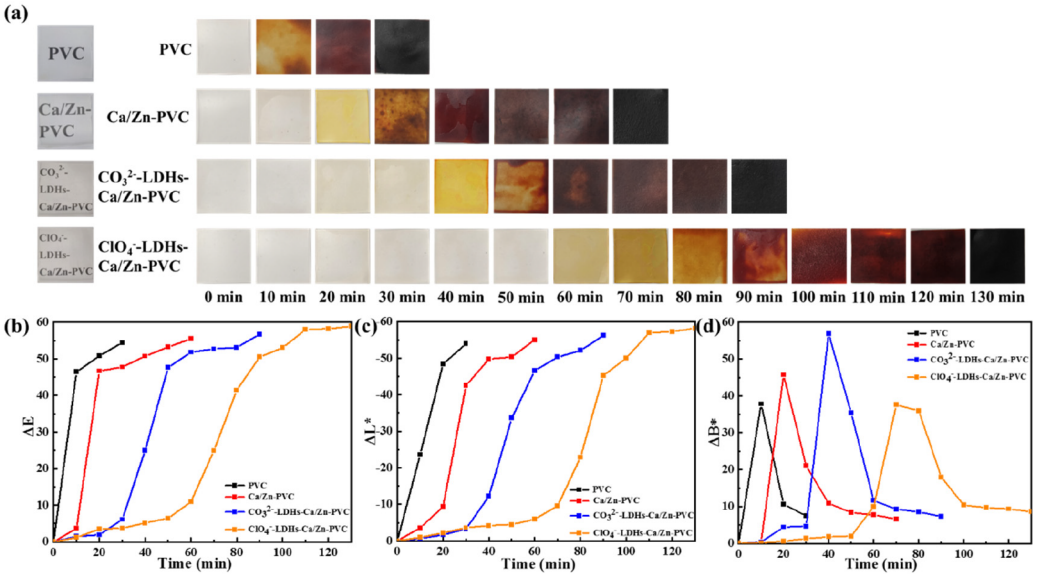

Figure 7. Pictures of the transparency of PVC sheets and the result in the PVC sheets recovered after heat-resistance test at 180 °C (a), and color change test results for ΔE (b), ΔL^* (c) and ΔB^* (d).

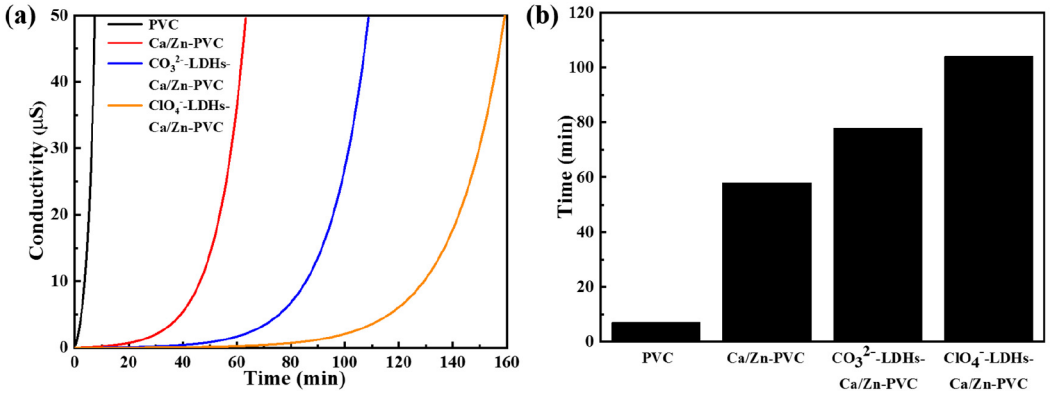

Figure 8. Representative Thermomat conductivity curves (a) and Congo red test result (b) of different PVC samples.

44.3% was detected in the temperature range of 50−800 °C for CO_3^{2-}-LDH, where three endothermic peaks were observed in the corresponding DTA curve. The first peak at 240 °C most likely corresponded to the release of absorbed water and intercalated water. The second one at 350 °C was due to the decomposition of intercalated carbonate anions and the dehydroxylation in the layers. The last peak at 410 °C reflected the dehydroxylation from the metal hydroxide layers and the extensive elimination of intercalated CO_3^{2-} in the interlayer. For ClO_4^--LDH, the mass loss increased to 49.2%, and the DTA curve of hydrotalcite after uptake of perchlorate ion showed one more endothermic peak at 445 °C compared with that of CO_3^{2-}-LDH, which was associated with the decompostion of ClO_4^- anions.

The pictures of the color change of PVC sheets recovered after the static thermal stability test at 180 °C are shown in Figure 7. Both the blank PVC and the PVC with added stabilizers had similar initial transparency. For blank PVC, after only 10 min the sample was colored brownish yellow, then becoming brown after 20 min, and finally blackened completely after 30 min. $Ca(St)_2$ and $Zn(St)_2$ can block the chain degradation of PVC to a certain extent. As expected, the starting time of the coloration of sample 2 was delayed obviously, appearing light-yellow after 30 min and turning black completely after 70 min. Sample 3 owing to the inhibitory effect of CO_3^{2-}-LDH had a better thermal resistance with 90 min stabilization time (blackened completely) compared with sample 2. More importantly, the ClO_4^- modified LDH endowed PVC with the best thermal stability with nearly 130 min stabilization time, and the yellowing time was extended to 60 min. The anion-exchange selectivity of LDH typically follows the sequence, $ClO_4^- < NO_3^- < Br^- < Cl^- < F^- < OH^- < SO_4^{2-} < HPO_4^{2-} < CO_3^{2-}$,[30] and compared with CO_3^{2-}, the ClO_4^- intercalated hydrotalcite more easily traps and exchanges the aggressive Cl^- anions produced by PVC degradation. ClO_4^- can also react with HCl to weaken its autocatalytic effect on the thermal aging of PVC. In view of the synergistic effect of ClO_4^- and LDH, the combination of recycled adsorbents and Ca/Zn based stabilizer had a stronger barrier effect on the chain degradation of PVC. Figure 7 further revealed the ΔE values of color change as a function on heat aging time. The ΔE values of all samples reached a constant value eventually, and the variation of ΔL^* was similar to that of ΔE, which corresponded to the gradual change of light color to dark color for all samples. The most apparent sign of thermal degradation of PVC is yellowing. It could be seen from Figure

https://doi.org/10.1021/acsomega.3c00176
ACS Omega 2023, 8, 17689−17698

7d that the time to obvious yellowing of ClO_4^--LDH−Ca/Zn-PVC was much longer than that of other samples, and the change of ΔB^* was very slow before 60 min. The introduction of ClO_4^--LDH hindered the removal of labile chlorine largely, thereby reducing the generation of conjugated polyenes and prolonging the time until onset of yellowing. All the observed trends were consistent with the discoloration test result of PVC sheets exhibited well in the digital photos.

A certain amount of HCl is released during the thermal degradation of PVC, leading to changes in the conductivity of the aqueous solution, which can be used to judge the thermal aging of PVC. The onset time of degradation is defined as the induction time (t_1) while the time required to achieve a conductivity of 50 $\mu s \cdot cm^{-1}$ is regarded as the stability time (t_2). Figure 8a displays the concentration of H^+ as a function of the degradation time. Obviously, ClO_4^--LDH−Ca/Zn-PVC had the highest ability to limit HCl release. The flattest trend from 0 to t_1 was exhibited for the curve of this sample, and it had t_1 and t_2 far higher than other sheets. Congo red test is one of the most effective methods for evaluating resistance against thermal degradation of PVC. Herein, the thermal stability time was defined as the time for the color to change from red to blue on Congo red test paper. As shown in Figure 8b, the stability time for the original PVC was only 7 min. The stability time was improved to 58 min when $Zn(St)_2$ and $Ca(St)_2$ stabilizers were incorporated. Notably, the discoloration time of Congo red test paper was delayed to 78 and 104 min, respectively, after further adding CO_3^{2-}-LDH and ClO_4^--LDH, consistent with the above conductivity results.

4. CONCLUSIONS

In this work, a new environmentally friendly route for recycling LDHs was proposed for sustainable utilization of a waste stream. Calcined hydrotalcite was used as an adsorbent for the removal of perchlorate ions from wastewater driven by the structure memory effect. Two different adsorption methods, ultrasound assistance and mechanical vibration, were compared in this experiment. A more favorable adsorption of ClO_4^- by the ultrasound-assisted sample was shown in the results. Compared with the mechanical vibration method, the maximum adsorption capacity of the adsorbents (291.89 mg/g) was increased, and the adsorption process was nicely fitted with the kinetic Elovich rate equation (R^2 = 0.992) and Langmuir adsorption model (R^2 = 0.996). Both the diffusion and adsorption of perchlorate anions were promoted more strongly under this technique, leading to a more efficient process for water remediation. Combined with the characterization data of the recycled adsorbent, the layered structure was restored successfully due to the structure memory effect and the perchlorate ions had been intercalated into the LDH layer. Further, the ClO_4^--LDH−Ca/Zn-PVC had better color retention, longer stability, and slower HCl release rate at high temperature, which was demonstrated by the experiments of long-term thermal aging, Congo red discoloration, and electrical conductivity, respectively. Compared with CO_3^{2-}-LDH, the recycled adsorbent endows PVC with better thermal stability and prolongs its service life.

AUTHOR INFORMATION

Corresponding Authors

Weifeng Song − *Global Innovation Center, Canadian General Tower Changshu Co. Ltd., Suzhou 215500, PR China*; Phone: +86-512-82359868-2092; Email: Albert.Song@cgtower.com; Fax: +86-512-82359858

Kangmin Niu − *School of Materials Science and Engineering, University of Science and Technology Beijing, Beijing 100083, PR China*; orcid.org/0000-0001-7554-7754; Phone: +86-18210136530; Email: niukm@ustb.edu.cn

Authors

Changwei Cui − *School of Materials Science and Engineering, University of Science and Technology Beijing, Beijing 100083, PR China; Global Innovation Center, Canadian General Tower Changshu Co. Ltd., Suzhou 215500, PR China*

Youhao Zhang − *Global Innovation Center, Canadian General Tower Changshu Co. Ltd., Suzhou 215500, PR China*

Michael A. Wladyka − *Global Innovation Center, Canadian General Tower Changshu Co. Ltd., Suzhou 215500, PR China*

Tianyu Wang − *School of Materials Science and Engineering, University of Science and Technology Beijing, Beijing 100083, PR China; Global Innovation Center, Canadian General Tower Changshu Co. Ltd., Suzhou 215500, PR China*

Complete contact information is available at: https://pubs.acs.org/10.1021/acsomega.3c00176

Notes

The authors declare no competing financial interest.

ACKNOWLEDGMENTS

Financial support from the Academic/Industry Cooperation Program of the Canadian General Tower and University of Science and Technology Beijing is gratefully acknowledged.

REFERENCES

(1) Cao, F.; Jaunat, J.; Sturchio, N.; Cancès, B.; Morvan, X.; Devos, A.; Barbin, V.; Ollivier, P. Worldwide occurrence and origin of perchlorate ion in waters: A review. *Sci. Total Environ.* **2019**, *661*, 737−749.

(2) Niziński, P.; Błażewicz, A.; Kończyk, J.; Michalski, R. Perchlorate-properties, toxicity and human health effects: an updated review. *Rev. Environ. Health* **2021**, *36*, 199−222.

(3) Hu, J.; Xian, Y.; Wu, Y.; Chen, R.; Dong, H.; Hou, X.; Liang, M.; Wang, B.; Wang, L. Perchlorate occurrence in foodstuffs and water: Analytical methods and techniques for removal from water-A review. *Food Chem.* **2021**, *360*, 130146.

(4) Wu, Q.; Zhang, T.; Sun, H.; Kannan, K. Perchlorate in tap water, groundwater, surface waters, and bottled water from China and its association with other inorganic anions and with disinfection byproducts. *Arch. Environ. Contam. Toxicol.* **2010**, *58*, 543−550.

(5) Walsh, M.; Walsh, M.; Ramsey, C.; Brochu, S.; Thiboutot, S.; Ampleman, G. Perchlorate contamination from the detonation of insensitive high-explosive rounds. *J. Hazard. Mater.* **2013**, *262*, 228−233.

(6) Comet, M.; Martin, C.; Schnell, F.; Schwartz, C.; Lallemand, B.; Galland, G.; Spitzer, D. Submicron potassium perchlorate: a key component to reach detonation in binary mixtures with titanium hydride. *Prop., Explos., Pyrotech.* **2021**, *46*, 1345.

(7) Nair, S.; Mathew, S.; Reghunadhan Nair, C. High energy materials as thermal decomposition modifiers of Ammonium perchlorate. *Mater. Today: Proc.* **2020**, *25*, 144−147.

(8) Acevedo-Barrios, R.; Olivero-Verbel, J. Perchlorate contamination: sources, effects, and technologies for remediation. *Rev. Environ. Contam. T.* **2021**, *256*, 103−120.

https://doi.org/10.1021/acsomega.3c00176
ACS Omega 2023, 8, 17689−17698

(9) Xie, Y.; Ren, L.; Zhu, X.; Gou, X.; Chen, S. Physical and chemical treatments for removal of perchlorate from water−A review. *Process Saf. Environ. Prot.* **2018**, *116*, 180−198.
(10) Xu, J.; Gao, N.; Zhao, D.; An, N.; Li, L.; Xiao, J. Bromate reduction and reaction-enhanced perchlorate adsorption by $FeCl_3$-impregnated granular activated carbon. *Water Res.* **2019**, *149*, 149−158.
(11) Wan, D.; Wu, L.; Liu, Y.; Zhao, H.; Fu, J.; Xiao, S. Adsorption of low concentration perchlorate from aqueous solution onto modified cow dung biochar: effective utilization of cow dung, an agricultural waste. *Sci. Total Environ.* **2018**, *636*, 1396−1407.
(12) Gao, M.; Wang, S.; Ren, Y.; Jin, C.; She, Z.; Zhao, Y.; Yang, S.; Guo, L.; Zhang, J.; Li, Z. Simultaneous removal of perchlorate and nitrate in a combined reactor of sulfur autotrophy and electrochemical hydrogen autotrophy. *Chem. Eng. J.* **2016**, *284*, 1008−1016.
(13) Kim, Y.; Lee, Y.; Choi, M. Complete degradation of perchlorate using Pd/N-doped activated carbon with adsorption/catalysis bifunctional roles. *Carbon* **2013**, *65*, 315−323.
(14) Xie, Y.; Wu, Y.; Qin, Y.; Yi, Y.; Liu, Z.; Lv, L.; Xu, M. Evaluation of perchlorate removal from aqueous solution by cross-linked magnetic chitosan/poly (vinyl alcohol) particles. *J. Taiwan Inst. Chem. Eng.* **2016**, *65*, 295−303.
(15) Mahmudov, R.; Huang, C. Perchlorate removal by activated carbon adsorption. *Sep. Purif. Technol.* **2010**, *70*, 329−337.
(16) Taviot-Guého, C.; Prévot, V.; Forano, C.; Renaudin, G.; Mousty, C.; Leroux, F. Tailoring hybrid layered double hydroxides for the development of innovative applications. *Adv. Funct. Mater.* **2018**, *28*, 1703868.
(17) Feng, J.; He, Y.; Liu, Y.; Du, Y.; Li, D. Supported catalysts based on layered double hydroxides for catalytic oxidation and hydrogenation: general functionality and promising application prospects. *Chem. Soc. Rev.* **2015**, *44*, 5291−5319.
(18) Allou, N.; Yadav, A.; Pal, M.; Goswamee, R. Biocompatible nanocomposite of carboxymethyl cellulose and functionalized carbon-norfloxacin intercalated layered double hydroxides. *Carbohydr. Polym.* **2018**, *186*, 282−289.
(19) Zhang, Z.; Qin, J.; Zhang, W.; Pan, Y.; Wang, D.; Yang, R. Synthesis of a novel dual layered double hydroxide hybrid nanomaterial and its application in epoxy nanocomposites. *Chem. Eng. J.* **2020**, *381*, 122777.
(20) Li, J.; Lin, K.; Luo, X.; Zhang, H.; Cheng, Y.; Li, X.; Liu, Y. Enhanced corrosion protection property of Li-Al layered double hydroxides (LDHs) film modified by 2-guanidinosuccinic acid with excellent self-repairing and self-antibacterial properties. *Appl. Surf. Sci.* **2019**, *480*, 384−394.
(21) Cao, Z.; Adnan, N.; Wang, G.; Rawal, A.; Shi, B.; Liu, R.; Liang, K.; Zhao, L.; Gooding, J.; Boyer, C.; Gu, Z. Enhanced colloidal stability and protein resistance of layered double hydroxide nanoparticles with phosphonic acid-terminated PEG coating for drug delivery. *J. Colloid Interface Sci.* **2018**, *521*, 242−251.
(22) Labuschagne, F.; Molefe, D.; Focke, W.; van der Westhuizen, I.; Wright, H.; Royeppen, M. Heat stabilising flexible PVC with layered double hydroxide derivatives. *Polym. Degrad. Stab.* **2015**, *113*, 46−54.
(23) Bai, S.; Chu, H.; Xiang, X.; Luo, R.; He, J.; Chen, A. Fabricating of $Fe_2O_3/BiVO_4$ heterojunction based photoanode modified with NiFe-LDH nanosheets for efficient solar water splitting. *Chem. Eng. J.* **2018**, *350*, 148−156.
(24) Asiabi, H.; Yamini, Y.; Shamsayei, M.; Tahmasebi, E. Highly selective and efficient removal and extraction of heavy metals by layered double hydroxides intercalated with the diphenylamine-4-sulfonate: A comparative study. *Chem. Eng. J.* **2017**, *323*, 212−223.
(25) Deng, H.; Yin, J.; Ma, J.; Zhou, J.; Zhang, L.; Gao, L.; Jiao, T. Exploring the enhanced catalytic performance on nitro dyes via a novel template of flake-network Ni-Ti LDH/GO in-situ deposited with Ag_3PO_4 NPs. *Appl. Surf. Sci.* **2021**, *543*, 148821.
(26) He, Y.; Wang, R.; Jiao, T.; Yan, X.; Wang, M.; Zhang, L.; Bai, Z.; Zhang, Q.; Peng, Q. Facile Preparation of Self-Assembled Layered Double Hydroxide-Based Composite Dye Films As New Chemical Gas Sensors. *ACS Sustain. Chem. Eng.* **2019**, *7*, 10888−10899.
(27) Kutlu, B.; Leuteritz, A.; Boldt, R.; Jehnichen, D.; Heinrich, G. Effects of LDH synthesis and modification on the exfoliation and introduction of a robust anion-exchange procedure. *Chem. Eng. J.* **2014**, *243*, 394−404.
(28) El Hassani, K.; Beakou, B.; Kalnina, D.; Oukani, E.; Anouar, A. Effect of morphological properties of layered double hydroxides on adsorption of azo dye Methyl Orange: a comparative study. *Appl. Clay Sci.* **2017**, *140*, 124−131.
(29) Cornejo, J.; Celis, R.; Pavlovic, I.; Ulibarri, M. Interactions of pesticides with clays and layered double hydroxides: a review. *Clay Miner.* **2008**, *43*, 155−176.
(30) Tamura, K.; Kawashiri, R.; Iyi, N.; Watanabe, Y.; Sakuma, H.; Kamon, M. Rosette-like layered double hydroxides: adsorbent materials for the removal of anionic pollutants from water. *ACS Appl. Mater. Interfaces* **2019**, *11*, 27954−27963.
(31) Ye, H.; Liu, S.; Yu, D.; Zhou, X.; Qin, L.; Lai, C.; Qin, F.; Zhang, M.; Chen, W.; Chen, W.; Xiang, L. Regeneration mechanism, modification strategy, and environment application of layered double hydroxides: Insights based on memory effect, Coord. *Chem. Rev.* **2022**, *450*, 214253.
(32) Mascolo, G.; Mascolo, M. On the synthesis of layered double hydroxides (LDHs) by reconstruction method based on the "memory effect". *Microporous Mesoporous Mater.* **2015**, *214*, 246−248.
(33) Kwon, D.; Kang, J.; An, S.; Yang, I.; Jung, J. Tuning the base properties of Mg−Al hydrotalcite catalysts using their memory effect. *J. Energy Chem.* **2020**, *46*, 229−236.
(34) Cardinale, A.; Fortunato, M.; Locardi, F.; Parodi, N. Thermal analysis of MgFe-Cl Layered doubled hydroxide (LDH) directly synthetized and produced "via memory effect". *J. Therm. Anal. Calorim.* **2022**, *147*, 5297−5302.
(35) Cosano, D.; Esquivel, D.; Romero-Salguero, F.; Jiménez-Sanchidrián, C.; Ruiz, J. Use of Raman spectroscopy to assess nitrate uptake by calcined LDH phases. *Colloids Surfaces A Physicochem. Eng. Asp.* **2020**, *602*, 125066.
(36) Miao, J.; Zhao, X.; Zhang, Y.; Lei, Z.; Liu, Z. Preparation of hollow hierarchical porous CoMgAl-borate LDH ball-flower and its calcinated product with extraordinary adsorption capacity for Congo red and methyl orange. *Appl. Clay Sci.* **2021**, *207*, 106093.
(37) Yang, Y.; Gao, N.; Deng, Y.; Zhou, S. Adsorption of perchlorate from water using calcined iron-based layered double hydroxides. *Appl. Clay Sci.* **2012**, *65*−*66*, 80−86.
(38) Lin, Y.; Fang, Q.; Chen, B. Perchlorate uptake and molecular mechanisms by magnesium/aluminum carbonate layered double hydroxides and the calcined layered double hydroxides. *Chem. Eng. J.* **2014**, *237*, 38−46.
(39) Liu, Y.; Liu, Y.; He, Q.; Guo, P.; Chen, J.; Wan, D.; Xiao, S. Utilizing the "memory effect" of bimetallic-supported hydrotalcites for adsorption and reduction of perchlorate in water. *Colloids Surfaces A Physicochem. Eng. Asp.* **2020**, *593*, 124641.
(40) Munonde, T.; September, N.; Mpupa, A.; Nomngongo, P. Two agitation routes for the adsorption of Reactive Red 120 dye on NiFe LDH/AC nanosheets from wastewater and river water. *Appl. Clay Sci.* **2022**, *219*, 106438.
(41) Yang, Z.; Wei, J.; Zeng, G.; Zhang, H.; Tan, X.; Ma, C.; Li, X.; Li, Z.; Zhang, C. A review on strategies to LDH-based materials to improve adsorption capacity and photoreduction efficiency for CO_2. *Coord. Chem. Rev.* **2019**, *386*, 154−182.
(42) Soltani, R.; Marjani, A.; Shirazian, S. A hierarchical LDH/MOF nanocomposite: single, simultaneous and consecutive adsorption of a reactive dye and Cr(vi). *Dalton Trans.* **2020**, *49*, 5323−5335.
(43) Hassani, A.; Khataee, A.; Karaca, S.; Karaca, C.; Gholami, P. Sonocatalytic degradation of ciprofloxacin using synthesized TiO_2 nanoparticles on montmorillonite. *Ultrason. Sonochem.* **2017**, *35*, 251−262.
(44) Karaca, M.; Kıranşan, M.; Karaca, S.; Khataee, A.; Karimi, A. Sonocatalytic removal of naproxen by synthesized zinc oxide nanoparticles on montmorillonite. *Ultrason. Sonochem.* **2016**, *31*, 250−256.

https://doi.org/10.1021/acsomega.3c00176
ACS Omega 2023, 8, 17689−17698

(45) Khataee, A.; Saadi, S.; Vahid, B.; Joo, S.; Min, B. Sonocatalytic degradation of Acid Blue 92 using sonochemically prepared samarium doped zinc oxide nanostructures. *Ultrason. Sonochem.* **2016**, *29*, 27−38.
(46) Iglesias, L.; Álvarez, M.; Chimentão, R.; Leganés, J.; Medina, F. On the role of ultrasound and mechanical stirring for iodide adsorption by calcined layered double hydroxides. *Appl. Clay Sci.* **2014**, *91*−*92*, 70−78.
(47) Zhang, W.; Liang, Y.; Wang, J.; Zhang, Y.; Gao, Z.; Yang, Y.; Yang, K. Ultrasound-assisted adsorption of Congo red from aqueous solution using $MgAlCO_3$ layered double hydroxide. *Appl. Clay Sci.* **2019**, *174*, 100−109.
(48) Szabados, M.; Varga, G.; Kónya, Z.; Kukovecz, Á.; Carlson, S.; Sipos, P.; Pálinkó, I. Ultrasonically-enhanced preparation, characterization of CaFe-layered double hydroxides with various interlayer halide, azide and oxo anions (CO_3^{2-}, NO_3^-, ClO_4^-). *Ultrason. Sonochem.* **2018**, *40*, 853−860.
(49) Khataee, A.; Arefi-Oskoui, S.; Samaei, L. ZnFe-Cl nanolayered double hydroxide as a novel catalyst for sonocatalytic degradation of an organic dye. *Ultrason. Sonochem.* **2018**, *40*, 703−713.
(50) Jiao, G.; Ma, J.; Li, Y.; Jin, D.; Ali, Z.; Zhou, J.; Sun, R. Recent advances and challenges on removal and recycling of phosphate from wastewater using biomass-derived adsorbents. *Chemosphere* **2021**, *278*, 130377.
(51) Dutta, T.; Kim, T.; Vellingiri, K.; Tsang, D.; Shon, J.; Kim, K.; Kumar, S. Recycling and regeneration of carbonaceous and porous materials through thermal or solvent treatment. *Chem. Eng. J.* **2019**, *364*, 514−529.
(52) Im, E.; Seo, H.; Kim, D.; Hyun, D.; Moon, G. Bimodally-porous alumina with tunable mesopore and macropore for efficient organic adsorbents. *Chem. Eng. J.* **2021**, *416*, 129147.
(53) Sanz-Pérez, E.; Dantas, T.; Arencibia, A.; Calleja, G.; Guedes, A.; Araujo, A.; Sanz, R. Reuse and recycling of amine-functionalized silica materials for CO_2 adsorption. *Chem. Eng. J.* **2017**, *308*, 1021−1033.
(54) Ou, B.; Wang, J.; Wu, Y.; Zhao, S.; Wang, Z. Efficient removal of Cr (VI) by magnetic and recyclable calcined CoFe-LDH/g-C_3N_4 via the synergy of adsorption and photocatalysis under visible light. *Chem. Eng. J.* **2020**, *380*, 122600.
(55) Jung, I.; Jo, Y.; Han, S.; Yun, J. Efficient removal of iodide anion from aqueous solution with recyclable core-shell magnetic Fe_3O_4@ Mg/Al layered double hydroxide (LDH). *Sci. Total Environ.* **2020**, *705*, 135814.
(56) Jia, Y.; Liu, Z. Preparation of borate anions intercalated MgAl-LDHs microsphere and its calcinated product with superior adsorption performance for Congo red. *Colloids Surfaces A Physicochem. Eng. Asp.* **2019**, *575*, 373−381.
(57) Mészáros, S.; Halász, J.; Kónya, Z.; Sipos, P.; Pálinkó, I. Reconstruction of calcined MgAl- and NiMgAl-layered double hydroxides during glycerol dehydration and their recycling characteristics. *Appl. Clay Sci.* **2013**, *80*−*81*, 245−248.
(58) Santos, R.; Gonçalves, R.; Constantino, V.; Santilli, C.; Borges, P.; Tronto, J.; Pinto, F. Adsorption of Acid Yellow 42 dye on calcined layered double hydroxide: Effect of time, concentration, pH and temperature. *Appl. Clay Sci.* **2017**, *140*, 132−139.
(59) Fan, L.; Yang, L.; Lin, Y.; Fan, G.; Li, F. Enhanced thermal stabilization effect of hybrid nanocomposite of Ni−Al layered double hydroxide/carbon nanotubes on polyvinyl chloride resin. *Polym. Degrad. Stab.* **2020**, *176*, 109153.
(60) Aisawa, S.; Nakada, C.; Hirahara, H.; Takahashi, N.; Narita, E. Preparation of dipentaerythritol-combined layered double hydroxide particle and its thermostabilizing effect for polyvinyl chloride. *Appl. Clay Sci.* **2019**, *180*, 105205.
(61) Guo, Y.; Zhang, Q.; Hu, Q.; Tian, W.; Leroux, F.; Tang, P.; Li, D.; Feng, Y. Size-dependent effect of MgAl-layered double hydroxides derived from $Mg(OH)_2$ on thermal stability of poly(vinyl chloride). *Mater. Today Commun.* **2021**, *29*, 102851.
(62) Guo, Y.; Leroux, F.; Tian, W.; Li, D.; Tang, P.; Feng, Y. Layered double hydroxides as thermal stabilizers for Poly(vinyl chloride): A review. *Appl. Clay Sci.* **2021**, *211*, 106198.
(63) Wypych, G. Principles of thermal degradation. *PVC Degradation and Stabilization*, 3rd ed.; Chemtec Publishing, 2015; pp 79−165.
(64) Wypych, G. Stabilization and stabilizers. *Handbook of Material Weathering*, 6th ed.; Elsevier, 2018; pp 785−827.
(65) Yan, J.; Yang, Z. Intercalated hydrotalcite-like materials and their application as thermal stabilizers in poly(vinyl chloride). *J. Appl. Polym. Sci.* **2017**, *134*, 44896.
(66) Wen, X.; Yang, Z.; Yan, J.; Xie, X. Green preparation and characterization of a novel heat stabilizer for poly(vinyl chloride)−hydrocalumites. *RSC Adv.* **2015**, *5*, 32020−32026.
(67) Li, S.; Feng, J.; Kou, X.; Zhao, Y.; Ma, X.; Wang, S. Al-Stabilized Double-Shelled Hollow CaO-Based Microspheres with Superior CO_2 Adsorption Performance. *Energy Fuel.* **2018**, *32*, 9692−9700.
(68) Meng, Z.; Fan, J.; Cui, X.; Yan, Y.; Ju, Z.; Lu, R.; Zhou, W.; Gao, H. Removal of perchlorate from aqueous solution using quaternary ammonium modified magnetic Mg/Al-layered double hydroxide. *Colloids Surfaces A Physicochem. Eng. Asp.* **2022**, *647*, 129111.
(69) Bumajdad, A.; Ali, S.; Mathew, A. Characterization of iron hydroxide/oxide nanoparticles prepared in microemulsions stabilized with cationic/non-ionic surfactant mixtures. *J. Colloid Interface Sci.* **2011**, *355*, 282−292.
(70) Yang, F.; Zhang, S.; Sun, Y.; Tsang, D.; Cheng, K.; Ok, Y. Assembling biochar with various layered double hydroxides for enhancement of phosphorus recovery. *J. Hazard. Mater.* **2019**, *365*, 665−673.
(71) Nguyen, D.; Nguyen, T.; Van, H.; Nguyen, V.; Nguyen, L.; Nguyen, T.; Nguyen, T.; Chu, T.; Nguyen, T.; Ha, L.; Vinh, N.; Thai, V.; Nguyen, V.; Nguyen, K.; Thang, P. Adsorption removal of ammonium from aqueous solution using Mg/Al layered double hydroxides-zeolite composite. *Environ. Technol. Inno.* **2022**, *25*, 102244.
(72) Byl, O.; Liu, J.; Wang, Y.; Yim, W.; Johnson, J.; Yates, J. Unusual hydrogen bonding in water-filled carbon nanotubes. *J. Am. Chem. Soc.* **2006**, *128*, 12090−12097.

https://doi.org/10.1021/acsomega.3c00176
ACS Omega 2023, 8, 17689−17698